Local pH Modulation during Electro-Enzymatic O2 Reduction: Characterization of the Influence of Ionic Strength by In Situ Fluorescence Microscopy

Hiu Mun Man, Ievgen Mazurenko, Hugo Le Guenno, Laurent Bouffier, Elisabeth Lojou, Anne de Poulpiquet

Local pH modulation during electro-enzymatic O_2 reduction: characterization of the influence of ionic strength by *in situ* fluorescence microscopy

Hiu Mun Man,[†] Ievgen Mazurenko,[†] Hugo Le Guenno,[+] Laurent Bouffier, [‡] Elisabeth Lojou,[†] and Anne de Poulpiquet[†,*]

[†] Aix-Marseille Univ., CNRS, Laboratory of Bioenergetics and Protein Engineering, UMR 7281, Mediterranean Institute of Microbiology, Marseille, France
[‡] Univ. Bordeaux, CNRS, Bordeaux INP, Institute of Molecular Sciences, UMR 5255, F-33400 Talence, France
[+] CNRS, Microscopy facility, FR 3479, Mediterranean Institute of Microbiology, Marseille, France
* adepoulpiquet@imm.cnrs.fr

ABSTRACT: Understanding how environmental factors affect the bioelectrode efficiency and stability is of uttermost importance to develop high-performance bioelectrochemical devices. By coupling fluorescence confocal microscopy *in situ* to electrochemistry, this work focuses on the influence of the ionic strength on electro-enzymatic catalysis. In this context, the 4 e^- / 4 H^+ reduction of O_2 into water by the bilirubin oxidase from *Myrothecium verrucaria* (*Mv*BOD) is considered as a model. The effects of salt concentration on the enzyme activity and stability were probed by enzymatic assays performed in homogeneous catalysis conditions and monitored by UV-vis absorption spectroscopy. They were also investigated in heterogeneous catalysis conditions by electrochemical measurements with *Mv*BOD immobilized at a graphite microelectrode. We demonstrate that the catalytic activity and stability of the enzyme both in solution and in the immobilized state at the bioelectrode were conserved with an electrolyte concentration of up to 0.5 M, both in a buffered and a non-buffered electrolyte. Relying on this, we used fluorescence confocal laser scanning microscopy coupled *in situ* to electrochemistry to explore the local pH of the electrolyte at the vicinity of the electrode surface at various ionic strengths and for several overpotentials. 3D proton depletion profiles generated by the interfacial electroenzymatic reaction were recorded in the presence of a pH sensitive fluorophore. These concentration profiles were shown to contract with increasing ionic strength, thus highlighting the need for a minimal electrolyte concentration to ensure availability of charged substrates at the electrode surface during electro-enzymatic experiments.

INTRODUCTION

Performing electrochemistry of redox enzymes requires combining the constraints associated with electrochemical techniques with those originating from biological molecules. This implies, on one hand, working in the presence of an electrolyte and immobilizing the enzymes at the electrode surface, thus exposing them to the electric field and the charges compensation at the electrochemical interface. On the other hand, the enzyme biological origin imposes mild working conditions, *e.g.* most of the times near neutral pH, ambient temperature and buffered solutions. Moreover, enzyme binding at the electrode must be soft enough to preserve the protein structure and its activity. In this context, the ionic strength of enzymatic and electrolytic solutions is a crucial parameter since it might influence on all aspects of the bioelectrocatalysis. It directly affects mass transport and substrate availability at the electrode interface. It dictates the conductivity of the solution thus affecting current transport. Purification procedures, in which proteins can be exposed to solutions of high ionic strengths,[1] suggest that enzyme activity and structure can be maintained upon exposure to high ionic strengths. Furthermore, high concentrations of salts are also frequently used for enzyme storage in the frozen state.

Systematic studies of the effect of ionic strength on enzyme activity and stability at the electrochemical interface are lacking, although they might be important especially in the case of enzyme physisorption. Bioelectrochemical experiments are generally performed in buffers with typical molarities around ~50-100 mM. Higher ionic strengths are sometimes used,[2-3] but this remains occasional since the rather low currents that are typically recorded result in negligible ohmic losses. Adding salts to the electrolyte is another way to tune the ionic strength. However, salts are not innocent in the electroenzymatic process since they can act as enzyme inhibitors or as activators.[4-8] They may also strongly impact the loading/desorption of the enzyme onto/from the electrochemical interface depending on the type of interactions involved.[9]

Most redox enzymes undergo proton coupled electron transfer.[10] Controlling proton availability at the electrochemical interface is thus of great importance to ensure efficient catalysis. Proton transport is also a key parameter in two-electrode devices such as EBFCs.[11] Furthermore, extreme pH values can lead to the irreversible enzyme denaturation requiring a control of the local pH environment. More generally, pH is important in electrocatalysis since the desired reaction or the parasitic reactions can be favored over one another depending on the pH value.[12] Among the recent techniques developed for mapping pH with high spatial and temporal resolution[13], *in situ* fluorescence confocal laser scanning microscopy (FCLSM) can be used to image proton diffusion profiles near the electrode surface. Early reported in the frame of abiotic catalysis during O_2 reduction or water oxidation[14-18], this method was recently shown to be suitable to characterize enzyme electrocatalysis.[6, 19]

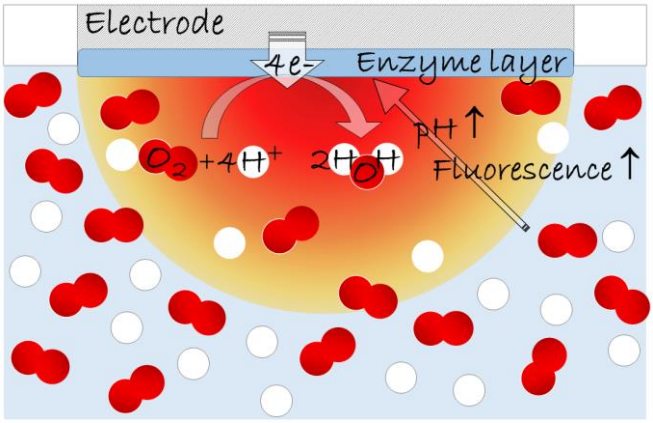

Scheme 1- Illustration of the measurements performed by *in situ* FCLSM. The O_2-reducing enzyme is immobilized at the graphite microelectrode, which directly provides the electrons necessary for the reaction. Simultaneously, proton consumption changes the pH in the diffusion layer, which in turn modulates the fluorescence of a pH-dependent reporter. The change of fluorescence intensity in the electrolyte volume is recorded by FCLSM. Radial cross sections of 3D images give the expansion of the hemispherical diffusion layer, here the "proton depletion layer", which is investigated at various potentials and ionic strengths.

In this work, we performed spatially-resolved pH measurements in order to determine to which extent the ionic strength can afford sufficient substrate availability for the enzymatic electrochemical reaction and alleviate any detrimental local pH. We selected the cathodic 4 electron-4 proton O_2 reduction reaction (ORR) by the bilirubin oxidase of *Myrothecium verrucaria* (*Mv*BOD). Its physisorption at a graphite microelectrode surface allows a direct electron pathway from the electrode to the mononuclear blue copper site (T1 Cu). Electrons are then transferred to the trinuclear Cu center where O_2 is reduced.[20-22] We first investigated the influence of ionic strength on the electrochemical signal and on the enzyme stability and activity in solution via UV-vis absorption spectroscopy. Then, to investigate the substrate transport properties, we recorded fluorescence at different focal planes localized close to the interface via *in situ* FCLSM in the presence of fluorescein as a pH-dependent fluorescent probe. We rebuilt 3D proton concentration profiles at the vicinity of the electrode surface during chronoamperometry experiments performed at different ionic strengths (Scheme 1). We especially highlight how the ionic strength strongly influences proton depletion profiles induced by the enzymatic reaction at graphite microelectrodes.

EXPERIMENTAL SECTION

Chemicals and Materials. 2,2'-azino-bis(3-ethylbenzothiazoline-6-sulfonic acid (ABTS), ammonium sulphate (AS), fluorescein, potassium phosphate monobasic (KH_2PO_4) and sulfuric acid (95 – 98 %), were obtained from Sigma Aldrich. Sodium hydroxide (50% w/w) came from Acros Organics and potassium phosphate dibasic (K_2HPO_4) from Fluka Analytical. Potassium phosphate buffer pH 6.0 (PB) was prepared by mixing K_2HPO_4 and KH_2PO_4 in appropriate ratios. All solutions were prepared with deionised water (Elga, U.K.). Bilirubin oxidase from *Myrothecium verrucaria* was received from Amano Enzyme (Japan) and used without further purification. The custom-built working electrode consists of a type-H graphite pencil rod (Ø = 0.3 mm) (Staedtler, Germany) inserted into a glass tube. The electrical connection is ensured by wrapping a thin wire around one end of the rod and coating with silver glue. The connection is wrapped with parafilm. The other end of the tube is filled with epoxy resin for insulation so that only the outermost surface of the electrode is in contact with the enzyme solution (during enzyme immobilization) or the electrolyte solution (in electrochemical measurements).

Bioelectrochemistry. Enzyme immobilisation was performed by dipping the graphite electrode into a 10 µM enzyme solution in 50 mM phosphate buffer (pH 6.0) (unless specified otherwise) for 10 minutes at 4°C. Bioelectrochemical experiments were performed in a conventional three-electrode cell, consisting of an Ag/AgCl/KCl sat. reference electrode (Ametek), a platinum wire as the counter electrode and the custom-made working electrode as described above. All potentials are referred to the Ag/AgCl/KCl sat. reference electrode. All experiments were performed at room temperature. The electrolyte solution (ammonium sulphate pH 5.4 (AS) or phosphate buffer pH 6.0 (PB), of different concentrations: 10, 50, 100 and 500 mM) was saturated with oxygen prior to electrochemical measurements. A continuous oxygen flow was maintained in the solution throughout the measurements. A constant potential of 0.0 V was applied for 60 s prior to cyclic voltammetry (CV) scans to avoid formation of an inactive resting enzyme form[5]. The CV potential window for the enzymatic O_2 reduction was set between +0.7 V and 0 V, with a scan rate of 0.005 V s^{-1}. The onset potentials were estimated as the potentials at which the current reaches 2% of its maximal value. The error bars were calculated from standard deviation divided by the square root of number of measurements (at least 3 replicates).

Modelling of the Cyclic Voltammetry (CV) Curves. Origin 8.5 was used to fit the electroenzymatic CV curves according to the formalism developed by Fourmond and Léger for irreversible reductive enzymatic catalysis (equation 1):[23]

$$i = \frac{i_{lim}^{red}}{a} \times \left[1 + \frac{1}{\beta d_0} ln \frac{a + \frac{k_{red}}{k^\circ_{OR}} b}{a + \frac{k_{red}}{k^\circ_{OR}} b \times \exp(\beta d_0)}\right] \quad (1)$$

Where a and b are defined for a one-electron transition by:

$$a = 1 + e_{OR} = 1 + \exp\left(\frac{F}{RT}(E - E^\circ{}_{Ox/R})\right) \quad (2)$$

And

$$b = e_{OR}^{\alpha} = e_{OR}^{1/2} = \exp\left(\frac{F}{2RT}(E - E^\circ{}_{Ox/R})\right) \quad (3)$$

F, R, and T have their usual meaning, $E^\circ{}_{Ox/R}$ is the formal potential for the one-electron conversion of the T1 copper center, i_{lim}^{red} is the value of the reductive limiting current, $k^\circ{}_{OR}$ is the rate constant of electron transfer at 0 overpotential for the one-electron conversion Ox/R, $k_{red}$is the rate constant of the associated chemical step and βd_0 is the dispersion parameter, which represents the distribution of enzyme orientations at the electrode surface.

In situ fluorescence microscopy during electrochemical experiments. The specially made opto-electrochemical cell comprising a 170 µm-thick optical window was positioned directly above the objective of a laser scanning confocal microscope Olympus FV1000-IX81. The working (WE) and reference electrodes are described above. The counter electrode is a titanium wire. Images were collected using an Olympus 20x objective MPLFLN (numerical aperture: 0.40). The electrochemical cell is mounted on the microscope stage thanks to a specifically 3D-printed holder, so that the WE can be positioned and focused manually in the x and y directions with good precision. The excited light travels through the objective to the WE surface, which is a few millimetres away from the optical window,

and then the emitted light is also collected through the objective (Scheme S1[24]). A precise focus of the electrode surface is obtained using the laser reflection mode of the microscope at the excitation wavelength λ = 543 nm with light collection in the range 500 - 580 nm through a 405/488 nm dichroic mirror filter. Afterwards, images are collected *in situ* during electrochemical measurements (chronoamperometry (CA)) in fluorescein-containing AS (initial pH = 5.4) or PB (initial pH = 5.8) solution at excitation wavelength λ = 488 nm. The light is collected in the range of 500-580 nm, after filtering with a 405/488/633 nm dichroic mirror. A constant potential is applied for 500 s and images are collected by scanning the WE from z = -20 (*i.e.* inside the electrode, z = 0 being the electrode surface position) to z = +300 µm along the z-axis (z_{step} = 5 µm) after the steady state has been reached. Measurements were performed in triplicates.

UV-vis absorption spectroscopy. Absorbance measurements were performed at a wavelength λ = 420 nm using a Varian Cary 50 UV-vis spectrophotometer (Varian, Agilent Technologies). The temperature was kept constant at 25 °C using a Varian Cary single cell Peltier accessory. The reaction rate was quantified by mixing 0.05 µM of *Mv*BOD in different concentrations of AS or PB (10, 50, 100 and 500 mM) with 1.5 mM ABTS. ABTS acts as the reducer in homogeneous conditions. It is transparent in its reduced form and turns blue when oxidized. The catalytic constant (k_{cat}) of *Mv*BOD was calculated by the equation 4:

$$k_{cat} = \frac{1}{[Enzyme]} \times \frac{1}{60 \times \varepsilon \times L} \times \left(\frac{dAbs}{dt}\right) \qquad (4)$$

where ε is ABTS molar absorptivity (ε(420 nm) = 36 mM^{-1} cm^{-1}) and L is the path length (L = 1 cm). Error bars were calculated from standard deviation divided by the square root of number of measurements, n = 3.

Fluorescence spectroscopy. Fluorescence spectra of fluorescein in different concentrations of AS (pH = 5.4) and PB (pH = 6.0) were recorded using a FluoroMax-4 spectrofluorometer (HORIBA Scientific). The excitation wavelength is 453 nm (slit width = 1 nm) and light is collected in the range of 470 – 600 nm (slit width: 1 nm). At least 3 replicates were performed.

Results and discussion

How the electrolyte concentration influences the enzyme (electro)activity. We first studied how varying the ionic strengths could affect enzymatic bio(electro)catalysis, and we probed the enzyme electroactivity (activity at the electrode surface by electrochemistry) and its specific activity in solution. One of the selected electrolytes, namely ammonium sulphate pH 5.4 (AS), is rather unusual in bioelectrochemistry. It has been selected here for its non-buffering properties allowing a wide pH modulation at the electrochemical interface, which is the basis of our fluorescence imaging strategy. It is also widely used at very high concentrations (~10 M) for salting out due to its non-denaturizing properties. We have shown previously that the enzyme activity and stability at the electrode and the CV trace of the electrochemical signature for O_2 reduction by *Mv*BOD were not affected by the addition of 75 mM AS to a 25 mM phosphate buffer electrolyte.[6] Moreover, the chosen pH is a compromise between enzyme optimal activity (pH 6.5)[25] and pH allowing fluorescence modulation with fluorescein. Indeed, the transition between the mono-anionic and the di-anionic forms of fluorescein which leads to the drastic increase of quantum yield from 0.37 to 0.93 is characterized by pKa = 6.4.[26] For comparison, experiments have also been performed in a more usual buffered electrolyte, namely phosphate buffer (PB) at pH 6.0, which is expected to reduce the influence of turnover-linked pH changes.

Enzyme specific activity. The specific homogeneous activity of *Mv*BOD recorded by UV-vis absorption spectroscopy only slighted decreased with increasing ionic strength. For instance, in PB the enzyme loses 22 % of its activity when PB concentration is increased from 10 to 500 mM, while in AS 16 % loss is observed when increasing electrolyte concentration from 100 to 500 mM. This might be explained by diminished electrostatic interactions at high ionic strengths between the enzyme and the ABTS substrate, which bears two sulfonic acid functions. While the first corresponds to a strong acid, the second protonation is characterized by pKa~2, meaning that ABTS global charge is -2 in our mild acidic pH conditions.[27] Our previous analysis have shown that while the protein global charge is negative at this pH, the zone surrounding the involved T1 Cu is positively charged. We can therefore assume that electrostatic forces contribute to the enzyme/substrate interactions. Increasing the salt concentration leads to ions interacting both with the protein and its substrate, so that the salt acts as an electrostatic shield decreasing the strength of these interactions. Interestingly also, quite similar activities are recorded in PB and AS, although the pH differs by 0.6 unit. We have measured the enzyme specific activity at different pH in both electrolytes at a given ionic strength (100 mM) and observed the classical bell-shaped evolution for the two of them (Figure S1). However, the maxima also differ by ~0.5 pH unit in the two electrolytes, being pH 6.5 and 6.0 in PB and AS, respectively.

Enzyme electroactivity. The evolution of electroactivity with electrolyte molarity is presented in Figure 1 (b and c). As anticipated, typical catalytic sigmoidal reduction curves are observed (Figure 1 b). When enzymes are immobilized at the electrode surface, the recorded current in the presence of substrate directly reflects the number of substrate molecules converted by the enzyme per unit of time at a given potential. This depends not only on the enzyme kinetics but also on the amount of enzyme and its interaction with the electrode surface. Therefore, the catalytic current is a complex combination of the quantity of immobilized enzyme, its specific activity in the immobilized form, and its ability to withdraw electrons from the electrode. We observe that electroactivity is typically lower in AS than in PB whatever the electrolyte concentration, while no obvious difference in specific activity between the two electrolytes could be recorded (Figure 1 a). Since we have shown previously that addition of AS in a PB buffered electrolyte did not affect enzyme electroactivity,[6] purely electrochemical factors must account for the differences. The influence of electrode surface size could be neglected since similar capacitive currents are recorded. On the contrary, electrode surface chemistry is expected to vary since the two electrolytes have a different pH value. Considering that the pKa of the graphite surface is 5.6,[28] the surface is slightly more negatively charged in the case of PB pH 6.0, which could induce a more favorable *Mv*BOD immobilization leading to higher currents. The modelling of CV curves indicates that the distribution of enzyme orientations is narrower in PB than in AS. More details can be found in SI. Consistently with the specific activity, electroactivity is maximal at pH 6.5 in PB and at pH 6.0 in AS, respectively (Figure S2). Interestingly also, while the specific activity is similar, the electroactivity remains smaller in AS than in PB whatever the pH. Therefore, not only the pH but also the nature of the electrolyte has

an influence on the magnitude of the electrochemical current and on the pH dependency of enzyme specific activity.

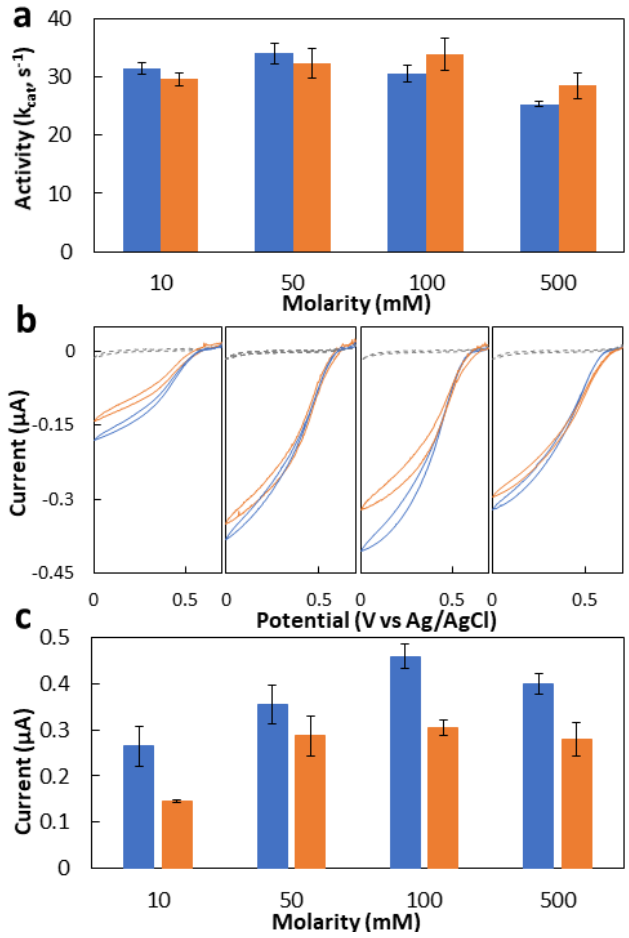

Figure 1. Influence of ionic strength on enzyme activity. (a) Specific activity (k_{cat}) of *Mv*BOD in different molarities of AS pH 5.4 (orange bar) and PB pH 6.0 (blue bar) solutions determined by UV-vis absorption spectroscopy. (b) Cyclic voltammograms (CVs) of ORR in increasing concentrations of AS pH 5.4 (orange line) and PB pH 6.0 (blue line) from left to right: 10 mM, 50 mM, 100 mM and 500 mM. The dotted lines indicate CVs recorded without enzyme. (c) Bar chart reporting the catalytic current at 0.0 V vs. Ag/AgCl against concentrations of AS pH 5.4 (orange) and PB pH 6.0 (blue). Experimental conditions: 25 °C, O_2-saturated solutions. In (b) and (c), the enzyme is physically adsorbed at graphite microelectrodes.

The trend is also slightly different in the two electrolytes. In AS, current is doubled when electrolyte concentration is increased from 10 to 50 mM. An increase is expected from the pure electrochemical viewpoint since at low ionic strength the increased electrolyte resistance might be responsible for lowering currents, but it should be negligible for such low currents. A more reasonable explanation is that the substrate availability decreases, as we will discuss later. For higher electrolyte concentrations, the catalytic current and thus the enzyme electroactivity is not varying much with increasing ionic strength (Figure 1c). A straightforward conclusion is that high electrolyte concentrations do not affect the activity of immobilized enzyme over short times (*i.e.* minutes). The influence on stability will be discussed hereafter. In PB, 75 % current increase is observed with increasing ionic strength from 10 to 100 mM, followed by a slight decrease at 500 mM (13 %). The maximal current is not obtained for the same electrolyte concentration as in AS but for close ionic strength values: indeed, given the composition of the two electrolytes, PB ionic strength I_{PB} is given by $I_{PB} = 1.25 \times C_{PB}$ at pH 6.0 while AS ionic strength I_{AS} is given by $I_{AS} = 3 \times C_{AS}$. The decrease observed afterwards might originate from a decreased activity of the immobilized enzyme, or a lower amount of enzyme being left at the electrode surface when the electrode is introduced in the electrolyte solution. We performed further experiments to clarify the relative contributions of the amount and activity of physisorbed enzyme in electroactivity. From the corresponding results, gathered in Figure S3, we discuss in SI the nature of interactions involved in enzyme attachment at graphite, with enzyme loading reaching an optimum at moderate ionic strengths. We conclude that the evolution of electroactivity with increasing ionic strength directly reflects the amount of immobilized enzyme.

A last interesting feature regarding the electrochemical signature is a small increase of ORR onset potential with increasing ionic strength (Figure 1b, Table S1). This onset is generally linked to the potential of T1 Cu since electrocatalysis is mainly considered to occur via direct electron transfer between the electrode and this copper site.[20] This observation could indicate a shift of the T1 Cu potential. The value of *Mv*BOD T1 Cu potential has been reported to be 670 mV vs. NHE at pH 7[29] and to vary with pH.[25, 30] An influence of ionic strength is not surprising since it affects ion activity, which in turn plays a role in the apparent standard potential. We give more details in SI. Another possibility is the decrease of activation overpotential with increasing ionic strength. This can be explained from the pure electrochemical viewpoint or from the catalytic side. On one hand, the additional energy necessary to activate the ions discharged at the required rate to promote the current flow would reduce with increasing ionic concentration. On the other hand, increased enzyme mobility at the interface with increasing ionic strength would account for an activation overpotential decrease. More details can also be found in SI.

To sum-up the experimental data of this first section, the main result is that both the enzyme activity and electroactivity of *Mv*BOD appear to be preserved when increasing the electrolyte concentration up to 0.5 M. Under these conditions, only a marginal decrease of activity was noticed.

Stability of the solubilized enzyme. We then explored the effect of ionic strength on the enzyme stability. Few studies on the topic can be found in the literature.[9, 31] Recently, Tsujimura *et al.* studied the effect of adding large quantities of ammonium sulphate (among other salts) on the heat stability of a FAD-dependent glucose dehydrogenase (GDH).[31] The enzyme was diluted in the electrolyte solution and the effect on the catalytic activity was determined. The GDH was stabilized by adding 0.5 M AS, showing enhanced residual activity after heat treatment at 50°C for 60 min. This was attributed to the compaction of the enzyme by kosmotropic anions (*i.e.* ions favoring order), which preserves its native structure. At a higher temperature (60°C), the stabilization was observed only for concentrations above 1.0 M. At both 50 and 60°C, no clear effect was observed for salt concentrations between 0.1 and 0.5 M. The influence of phosphate for heat-stabilization was also studied and no clear effect was observed for concentrations below 1 M. As far as we know, the influence of these ions on the stability at much lower temperatures (RT or 25°C) has not been investigated.

First, we investigated how incubating the enzyme in solutions of varying ionic strength could affect its stability in solution. We diluted the enzyme in solutions of varying ionic strengths and activity towards ORR in homogeneous catalysis was probed by UV-vis absorption spectroscopy before and after 1-hour incubation at room temperature. Enzymatic assays were performed in classical conditions (100 mM PB pH 6.0, ABTS as the electron donor). First of all, no clear influence of the ionic strength on the residual activity was observed (Figure 2). Moreover, the preservation of activity is similar in the PB and in the AS solutions, while the GDH showed a better stability in AS.[31] Since AS is more acidic here, we also performed the same experiment at different pH in both electrolytes at a given ionic strength (100 mM). The same tendency was observed in both electrolytes (Figure S4), with a slight and linear increase of stability with increasing pH: the residual activity increases from 64% at pH 5.0 to 74% at pH 6.5 and from 69% at pH 6.0 to 76% at pH 7.5 in AS and in PB, respectively. This shows that while the electrolyte acidity slightly decreases the enzyme stability, the electrolyte nature is contributing only weakly.

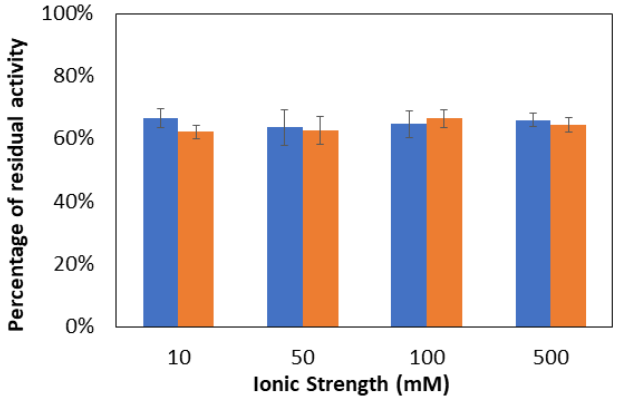

Figure 2. Influence of ionic strength of storage solutions on enzyme stability. Percentage of conserved specific activity (k_{cat}) of *Mv*BOD determined by UV-vis absorption spectroscopy after storage at RT for 1 hour at 5 µM in different molarities of AS pH 5.4 (orange bar) and PB pH 6.0 (blue bar) solutions. Experimental conditions: 25 °C, O_2-saturated solutions.

Stability of the immobilized enzyme. Stability of the electroenzymatic ORR results from both the biochemical stability of the immobilized enzyme and the mechanical stability of its immobilization at the electrode. The bioelectrode stability, illustrated by the evolution of signal intensity with cycling time, is similar regardless of the electrolyte concentration (Figure 3) or its nature (Figure S5). The decrease is faster in the first cycles before the current tends to stabilize, with 60% of the initial intensity that is maintained after 10 cycles (~45 minutes). A fast equilibrium between adsorbed/desorbed enzyme might be established before the cycling has started whatever the ionic strength. Therefore, the major contribution to the decrease of the response must be related to the intrinsic stability of the adsorbed enzyme, meaning that the immobilized enzyme is as stable as in solution on this timescale. More interesting is the absence of significant difference between the two electrolytes, although pH is expected to change cyclically over time at the electrode surface in the non-buffered electrolyte,[6] which could result in damages on the exposed enzyme at the interface. This experiment suggests that either a balance between an increased stability and a decreased specific activity of enzyme at higher pH is obtained, or enzyme immobilization somehow prevents the damaging effects of pH change.

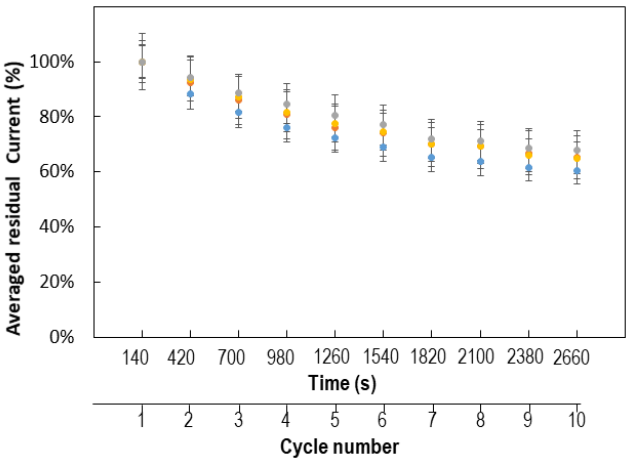

Figure 3. Influence of ionic strength on bioelectrode stability in phosphate buffer pH 6.0. *Mv*BOD is physisorbed at the graphite electrode surface and the potential is cycled between 0.7 and 0.0 V vs. Ag/AgCl. The graph shows the percentage deviation of current at 0.0 V vs. Ag/AgCl against time and cycle number in different concentrations of electrolyte: 10 mM (blue dots), 50 mM (orange dots), 100 mM (yellow dots) and 500 mM (grey dots), respectively.

Stability of enzyme immobilization. The bioelectrode stability is not decreasing with increasing ionic strengths, possibly due to the establishment of an equilibrium before the electrochemical measurements. However, if enzyme immobilization is relying on pure electrostatic interactions, the catalytic signal is expected to decrease upon a brutal increase of ionic strength. For example, Zebda and co-workers showed that adsorption/desorption of *Trametes versicolor* laccase on amino-functionalized carbon nanotubes could be tuned by changing the ionic strength in the electrolyte. In particular, adding 500 mM $NaHCO_3$ to the buffer provoked the loss of 65% of the immobilized laccase.[9] In a further experiment, we added a concentrated electrolyte in the electrochemical cell during the measurement (Figure S6). In a first step the electrolyte concentration was increased from 50 to 100 mM, and in a second step to 500 mM. Results slightly differ between the two electrolytes. In PB, 92% and 75% of initial current are conserved in the first and second steps, respectively. In AS even more electroactivity is conserved (95% in the first step and 80% after the second one). This observation, combined with what we have discussed above, tends towards the conclusion that various interactions are involved in the physisorption of *Mv*BOD at the graphite electrode surface. Again, the major conclusion of these experiments is that the intrinsic stability of the enzyme bound to the electrode surface is only marginally affected when increasing the electrolyte concentration up to 0.5 M. Therefore, there is no obstacle to studying the behavior of the enzymatic electrode at these electrolyte concentrations over the timescale required for the proposed *in-situ* FCLSM coupling method.

3D-Mapping of the electrode/electrolyte interface by fluorescence confocal laser scanning microscopy. The next step towards the understanding of ORR by *Mv*BOD was to investigate proton availability at the vicinity of the electrode surface with varying ionic strength. For this purpose, we selected fluorescein, which is a well-known pH-dependent fluorophore. Its pKa matches well with the *Mv*BOD optimum activity, whereas its electro-inactivity in the desired potential range

makes it suitable to evidence pH changes at the electrochemical interface during enzymatic ORR.[6] Using fluorescence spectroscopy control experiments we checked that the fluorescein quantum yield is not affected by increasing sulphate or phosphate anions concentrations, nor by the presence of O_2 (Figure S7 & S8). Fluorescence intensity evolution with varying ionic strength shows no specific trend, suggesting that AS or PB do not particularly quench the fluorescence of fluorescein. This latter is also the same under pure O_2, pure N_2 or air, showing that O_2 quenching is negligible. To give a comparison, addition of 20 mM iodide to the same fluorescein solution leads to a 20% fluorescence intensity decrease (Figure S9 and Table S2).

In the *in-situ* FCLSM mode, the 3-electrode electrochemical cell is placed on the stage of an inverted confocal microscope and the working electrode faces the objective. Several potential steps were applied at the electrode for the four electrolyte concentrations, and the current was recorded over time. Simultaneously, fluorescence was recorded in the electrolyte solution in planes parallel to the electrode surface after the steady-state (indicated by a current remaining constant) was reached. The experiment was first performed at a potential of + 0.6 V vs. Ag/AgCl, *i.e.* above the catalysis onset and close to the open circuit potential of the bioelectrode, to confirm the absence of spurious fluorescence modulation at the interface. Then, potentials of + 0.4 V, + 0.2 V and 0.0 V vs. Ag/AgCl at which enzymatic O_2 reduction readily occurs were applied. Decreasing the potential increases the driving force of the reaction and the number of enzymes participating in catalysis.[32] In each case, the focal plane was incrementally moved away from the electrode surface, allowing to rebuild the 3D fluorescence profiles at various ionic strengths. Radial cross sections of these 3D images recorded in PB and AS are shown in Figure 4 and Figure 5, respectively. Fluorescein fluorescence quantum yield drastically increases from 37% in the mono-anionic form to 93% in the di-anionic form. The maximal fluorescence intensity reflects therefore the maximal pH, so that the fluorescence profiles correspond to the proton depletion at the electrode.

The electrode/electrolyte boundary can be clearly distinguished: the electrolyte appears brighter than the electrode due to the residual fluorescence of fluorescein at the initial pH. The conductive area can also be discerned as it causes a kind of "shadow" in the electrolyte. This could result from optical effects due to the darker carbon material. A first key observation is that the electrolyte fluorescence is homogeneous and no modulation at the electrode interface can be observed at 0.6 V vs. Ag/AgCl, neither in PB (Figure 4) nor in AS (Figure 5). This is consistent with no reaction occurring at this applied potential.

In PB, for electrolyte concentrations above 10 mM, fluorescence intensity change at the electrode surface is very low (Figure 4), although the recorded currents prove that enzymatic catalysis is taking place (data not shown). Only the electrode "shadow" is disappearing at lower potentials. By contrast, in the low supported 10 mM PB electrolyte, a clear fluorescence modulation related to enzymatic electrocatalysis is seen at + 0.4, + 0.2 and 0.0 V vs. Ag/AgCl. The interfacial fluorescence intensity also increases with decreasing applied potentials but its shape and expansion are difficult to quantify. However, it is striking that small buffer concentrations are not sufficient to avoid pH modulation at the electro-enzymatic interface. The fluorescence modulation is expected to be larger in AS than in PB. Indeed, the homogeneous reaction taking place in PB with the buffer ensures a quasi-constant pH at the interface. Nevertheless, we have shown previously that pH changes caused by the enzymatic reaction at macroelectrodes could be recorded even in the presence of 25 mM buffer.[6] However, they are more difficult to evidence at smaller electrodes where the enzymatic currents, and thus the proton consumption rate, are lower. Moreover, to remain in the buffer range of PB a slightly higher initial pH than in AS was chosen (5.8 instead of 5.4). Since this is closer to the fluorescein pKa, the same pH increase results in a lower fluorescence modulation.

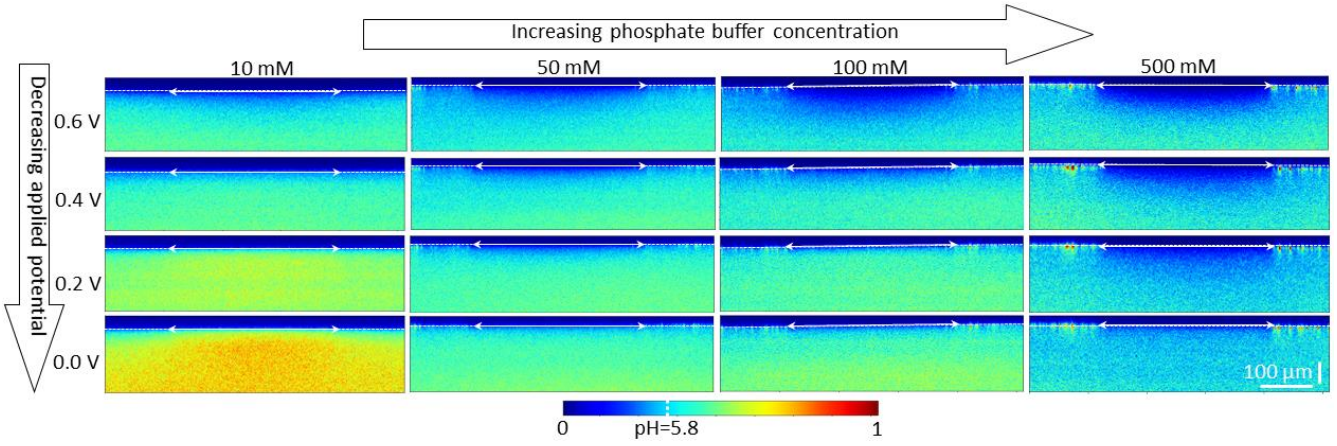

Figure 4. Radial cross sections of the proton depletion profiles at the enzymatic electrode during chronoamperometric measurements at a constant potential (from top to bottom: + 0.6 V, +0.4 V, +0.2 V and 0.0 V (*vs.* Ag/AgCl)) in increasing concentrations of PB pH 5.8 (from left to right: 10 mM, 50 mM, 100 mM and 500 mM). The dotted line indicates the electrode/electrolyte boundary; the arrow indicates the conductive surface. Fluorescence intensity scale and an indication of pH values are given at the bottom. Electrolyte: PB, initial pH = 5.8, 10 µM fluorescein, quiescent electrolyte under air atmosphere. $\lambda_{excitation}$ = 488 nm

In the AS electrolyte, the fluorescence intensity increases at higher overpotentials with a much larger amplitude as illustrated by the marked red color observed especially with the 10 mM and the 50 mM solutions (Figure 5). It is noteworthy that the microscope parameters were kept constant and that the same look-up table was used to encode the fluorescence intensity in Figures 4 and 5. To help the reader, we indicate on the fluorescence scale the initial pH values. The images show a maximal fluorescence intensity at the electrode/electrolyte interface, indicative of proton consumption linked to the localized

enzymatic O_2 reduction. An extended quasi-hemispherical fluorescence gradient is observed at low ionic strengths which indicates that proton depletion is expanding in the electrolyte in the direction of the electric field. This is in full agreement with the fact that protons which are positively charged migrate under the influence of the electric field which is oriented from the cathode (i.e. the working electrode) to the anode (i.e. the counter electrode). In the close vicinity of the electrode surface, the electric field is perpendicular to the surface and directed downwards, meaning towards the bulk electrolyte. The negatively charged mono- and di-anionic forms of fluorescein should migrate in the reverse direction. However, it has been previously shown that when using a 10 µM solution, fluorescein migration can be neglected from electrolyte concentrations as low as 1 mM,[18] which is the case in our experimental conditions.

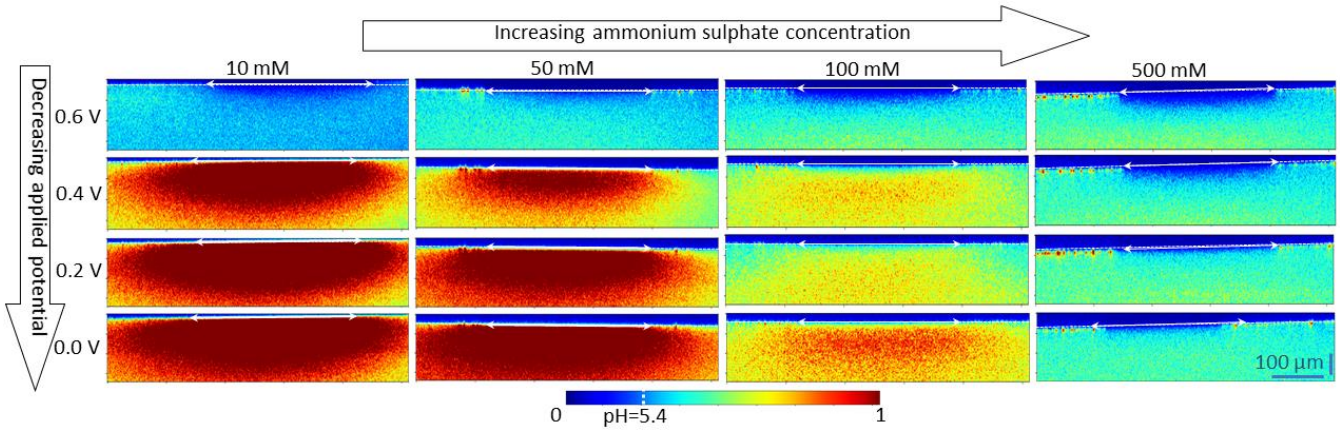

Figure 5. Radial cross sections of the proton depletion profiles at the enzymatic electrodes during chronoamperometric measurements at a constant potential (from top to bottom: + 0.6 V, +0.4 V, +0.2 V and 0.0 V (*vs.* Ag/AgCl)) in increasing concentrations of AS pH 5.4 (from left to right: 10 mM, 50 mM, 100 mM and 500 mM). The dotted line indicates the electrode/electrolyte interface; the arrow indicates the conductive surface. Fluorescence intensity scale and an indication of pH values are given at the bottom. Electrolyte: AS, initial pH = 5.4, 10 µM fluorescein, quiescent electrolyte under air atmosphere. $\lambda_{excitation}$ = 488 nm

Like in the PB electrolyte, the expansion of the depletion layer is maximal at 10 mM electrolyte concentration, where the catalytic current has been shown to be minimal. On the contrary, the depletion layer is contracted at high ionic strengths. Again, this agrees fully with the fact that the numerous electrolyte ions ensure the current transport via migration, which in turns decreases the migration of the charged species involved in the electroenzymatic process (*i.e.* the protons). The extension of the depletion layer also increases in both axial and lateral directions with increasing overpotentials. At 0.0 V, the depth of the depletion layer can be estimated to increase from 100 µm in the case of the 500 mM electrolyte (which eventually masks the shadow of the electrode), to over 300 µm for solution molarities below 100 mM. From these data, the ionic strength required to ensure substrate availability at the electrode surface can be anticipated. This unprecedented level of information is essential in the case of H_2/O_2 EBFCs where protons ensure the current transport while being involved both in anodic and cathodic reactions. In this specific case, we have investigated H^+ availability, which evidences drastic pH changes at the electrode interface. Moreover, since fluorophores sensitive to almost any chemicals are available we can envision doing the same for more complex substrates.

CONCLUSION

We described here the use of *in situ* FCLSM during electrochemical experiments to characterize the influence of the ionic strength on substrate mass transport at the bio-electrochemical interface. As a model, we selected the enzymatic O_2 reduction to water by *Mv*BOD, which involves the consumption of the H^+ charged species. We clearly evidenced an expansion of the proton depletion layer at the interface with decreasing ionic strength. Just as the diffusion layer, the length of this depletion layer will affect the current densities and can become limiting especially at high electrode reaction rates. Moreover, the required minimal electrolyte concentration should not affect the intensity and stability of the bioelectrochemical signal. To estimate a reasonable ionic strength compromise and ensure the validity of our FCLSM study, we examined the influence of electrolyte concentrations on the activity and stability of 1) the enzyme and 2) the enzymatic bioelectrode for the cathodic O_2 reduction. We showed that neither a marked inhibition nor a destabilization of the enzyme or the bioelectrode can be observed in electrolyte concentrations up to 0.5 M. However, more exhaustive studies of the influence of electrolyte for bioelectrode stabilization/destabilization would require to deal with even higher concentrations in the molar range, like those mentioned for example by N. Nemoto *et al.*[31]. Despite that, this study provides a new methodology to investigate the distance-dependent modulation of the electrolyte chemical composition during bioelectrocatalysis. Since this directly affects the current density generated in two-electrode devices like EBFCs, the method can be a key characterization to improve and optimize their performances, while the results presented here bring new qualitative clues in order to address bioelectrocatalysis in unusual conditions like more saline environments. Moreover, although this study focused on the proton transport, the observed behavior can be transposed to some extent to that of any charged species. In the case of EBFCs, studying how ionic strength influences the transport properties of ion exchange membrane, which separates physically the anode and the cathode, will also be of major interest. Finally, in this case of an enzymatic reduction reaction that is linked to a pH increase, pH changes at the electrode interface are shown not to be the major destabilizing factor.

ASSOCIATED CONTENT

Supporting Information Scheme S1. Experimental setup; Figure S1. Dependence of enzyme specific activity on pH; Figure S2. Dependence of enzyme electroactivity on pH; Table S1. Catalytic onset potential; Figure S3. Enzyme loading; Figure S4. Influence of pH on the stability of enzyme in solution; Figure S5. Stability of immobilized enzymes; Figure S6. Stability of enzyme immobilization; Figure S7. Influence of phosphate or sulphate anions on fluorescein fluorescence; Figure S8. Influence of O_2 on fluorescein fluorescence; Figure S9 & table S2. Quenching of the fluorescein fluorescence by iodide

The Supporting Information is available free of charge on the ACS Publications website.

AUTHOR INFORMATION

Corresponding Author

* adepoulpiquet@imm.cnrs.fr

Author Contributions

All authors have given approval to the final version of the manuscript

ACKNOWLEDGMENT

The authors gratefully acknowledge CNRS Mission for Interdisciplinarity for funding under the grant "Défi Imag'In MOMA", Frédérique Berger from Aix-Marseille University for the design and fabrication of the electrochemical cell enabling fluorescence microscopy measurements, and Amano Japan for kindly providing *Myrothecium verrucaria* Bilirubin oxidase. They also thank Dr. B. Goudeau (ISM, Bordeaux, France) and Dr. Artemis Kosta (IMM, Marseille, France) for technical support and Pr. T. Doneux (ULB, Brussels, Belgium) for fruitful discussion. H. M. Man acknowledges Région Sud and HySEAS for funding her PhD thesis.

REFERENCES

1. Duong-Ly, K. C.; Gabelli, S. B., Salting out of Proteins Using Ammonium Sulfate Precipitation. In *Laboratory Methods in Enzymology: Protein, Pt C*, Lorsch, J., Ed. 2014; Vol. 541, pp 85-94.

2. Tsujimura, S.; Murata, K.; Akatsuka, W., Exceptionally High Glucose Current on a Hierarchically Structured Porous Carbon Electrode with "Wired" Flavin Adenine Dinucleotide-Dependent Glucose Dehydrogenase. *J. Am. Chem. Soc.* **2014,** *136* (41), 14432-14437.

3. Sakai, H.; Nakagawa, T.; Tokita, Y.; Hatazawa, T.; Ikeda, T.; Tsujimura, S.; Kano, K., A high-power glucose/oxygen biofuel cell operating under quiescent conditions. *Energy Environ. Sci.* **2009,** *2* (1), 133-138.

4. Hirose, J.; Inoue, K.; Sakuragi, H.; Kikkawa, M.; Minakami, M.; Morikawa, T.; Iwamoto, H.; Hiromi, K., Anions binding to bilirubin oxidase from *Trachyderma tsunodae* K-2593. *Inorganica Chim. Acta* **1998,** *273* (1-2), 204-212.

5. de Poulpiquet, A.; Kjaergaard, C. H.; Rouhana, J.; Mazurenko, I.; Infossi, P.; Gounel, S.; Gadiou, R.; Giudici-Orticoni, M. T.; Solomon, E. I.; Mano, N.; Lojou, E., Mechanism of Chloride Inhibition of Bilirubin Oxidases and Its Dependence on Potential and pH. *ACS Catal.* **2017,** *7* (6), 3916-3923.

6. Tassy, B.; Dauphin, A. L.; Man, H. M.; Le Guenno, H.; Lojou, E.; Bouffier, L.; de Poulpiquet, A., In Situ Fluorescence Tomography Enables a 3D Mapping of Enzymatic O_2 Reduction at the Electrochemical Interface. *Anal. Chem.* **2020,** *92* (10), 7249-7256.

7. del Barrio, M.; Sensi, M.; Fradale, L.; Bruschi, M.; Greco, C.; de Gioia, L.; Bertini, L.; Fourmond, V.; Leger, C., Interaction of the H-Cluster of FeFe Hydrogenase with Halides. *J. Am. Chem. Soc.* **2018,** *140* (16), 5485-5492.

8. Larsson, T.; Lindgren, A.; Ruzgas, T.; Lindquist, S. E.; Gorton, L., Bioelectrochemical characterisation of cellobiose dehydrogenase modified graphite electrodes: ionic strength and pH dependences. *J. Electroanal. Chem.* **2000,** *482* (1), 1-10.

9. El Ichi-Ribault, S.; Zebda, A.; Tingry, S.; Petit, M.; Suherman, A. L.; Boualam, A.; Cinquin, P.; Martin, D. K., Performance and stability of chitosan-MWCNTs-laccase biocathode: Effect of MWCNTs surface charges and ionic strength. *J. Electroanal. Chem.* **2017,** *799*, 26-33.

10. Dempsey, J. L.; Winkler, J. R.; Gray, H. B., Proton-Coupled Electron Flow in Protein Redox Machines. *Chem. Rev.* **2010,** *110* (12), 7024-7039.

11. Oliot, M.; Galier, S.; de Balmann, H. R.; Bergel, A., Ion transport in microbial fuel cells: Key roles, theory and critical review. *Appl. Energy* **2016,** *183*, 1682-1704.

12. Edwardes Moore, E.; Cobb, S. J.; Coito, A. M.; Oliveira, A. R.; Pereira, I. A. C.; Reisner, E., Understanding the local chemical environment of bioelectrocatalysis. *Proc. Natl. Acad. Sci. U. S. A.* **2022,** *119* (4), e2114097119.

13. Monteiro, M. C. O.; Koper, M. T. M., Measuring local pH in electrochemistry. *Curr. Opin. Electrochem.* **2021,** *25*, 100649.

14. Cannan, S.; Macklam, I. D.; Unwin, P. R., Three-dimensional imaging of proton gradients at microelectrode surfaces using confocal laser scanning microscopy. *Electrochem. Comm.* **2002,** *4* (11), 886-892.

15. Rudd, N. C.; Cannan, S.; Bitziou, E.; Ciani, L.; Whitworth, A. L.; Unwin, P. R., Fluorescence confocal laser scanning microscopy as a probe of pH gradients in electrode reactions and surface activity. *Anal. Chem.* **2005,** *77* (19), 6205-6217.

16. Engstrom, R. C.; Ghaffari, S.; Qu, H. W., Fluorescence imaging of electrode solution interfacial processes. *Anal. Chem.* **1992,** *64* (21), 2525-2529.

17. Bowyer, W. J.; Xie, J.; Engstrom, R. C., Fluorescence imaging of the heterogeneous reduction of oxygen. *Anal. Chem.* **1996,** *68* (13), 2005-2009.

18. Pande, N.; Chandrasekar, S. K.; Lohse, D.; Mul, G.; Wood, J. A.; Mei, B. T.; Krug, D., Electrochemically Induced pH Change: Time-Resolved Confocal Fluorescence Microscopy Measurements and Comparison with Numerical Model. *J. Phys. Chem. Lett.* **2020,** *11* (17), 7042-7048.

19. Bollella, P.; Melman, A.; Katz, E., Operando Local pH Mapping of Electrochemical and Bioelectrochemical Reactions Occurring at an Electrode Surface: Effect of the Buffer Concentration. *ChemElectroChem.* **2021,** *8* (20), 3923-3935.

20. Mano, N.; de Poulpiquet, A., O-2 Reduction in Enzymatic Biofuel Cells. *Chem. Rev.* **2018,** *118* (5), 2392-2468.

21. Hitaishi, V. P.; Mazurenko, I.; Harb, M.; Clement, R.; Taris, M.; Castano, S.; Duche, D.; Lecomte, S.; Ilbert, M.; de Poulpiquet, A.; Lojou, E., Electrostatic-Driven Activity, Loading, Dynamics, and Stability of a Redox Enzyme on

Functionalized Gold Electrodes for Bioelectrocatalysis. *ACS Catal.* **2018,** *8* (12), 12004-12014.
22. Gutierrez-Sanchez, C.; Ciaccafava, A.; Blanchard, P. Y.; Monsalve, K.; Giudici-Orticoni, M. T.; Lecomte, S.; Lojou, E., Efficiency of Enzymatic O_2 Reduction by *Myrothecium verrucaria* Bilirubin Oxidase Probed by Surface Plasmon Resonance, PMIRRAS, and Electrochemistry. *ACS Catal.* **2016,** *6* (8), 5482-5492.
23. Fourmond, V.; Leger, C., Modelling the voltammetry of adsorbed enzymes and molecular catalysts. *Curr. Opin. Electrochem.* **2017,** *1* (1), 110-120.
24. de Poulpiquet, A.; Goudeau, B.; Garrigue, P.; Sojic, N.; Arbault, S.; Doneux, T.; Bouffier, L., A snapshot of the electrochemical reaction layer by using 3 dimensionally resolved fluorescence mapping. *Chem. Sci.* **2018,** *9* (32), 6622-6628.
25. Cracknell, J. A.; McNamara, T. P.; Lowe, E. D.; Blanford, C. F., Bilirubin oxidase from Myrothecium verrucaria: X-ray determination of the complete crystal structure and a rational surface modification for enhanced electrocatalytic O_2 reduction. *Dalton Trans.* **2011,** *40* (25), 6668-6675.
26. Sjoback, R.; Nygren, J.; Kubista, M., Absorption and Fluorescence Properties of Fluorescein. *Spectrochim. Acta - A : Mol. Biomol. Spectrosc.* **1995,** *51* (6), L7-L21.
27. Scott, S. L.; Chen, W. J.; Bakac, A.; Espenson, J. H., Spectroscopic parameters, electrode potentials, acid ionization constants, and electron-exchange rates of the 2,2'-azinobis(3-ethylbenzothiazoline-6-sulfonate) radical and ions. *J. Phys. Chem.* **1993,** *97* (25), 6710-6714.
28. Armstrong, F. A.; Cox, P. A.; Hill, H. A. O.; Lowe, V. J.; Oliver, B. N., Metal ions and complexes as modulators of protein interfacial electron tranport at graphite electrodes. *J. Electroanal. Chem.* **1987,** *217* (2), 331-366.
29. Shleev, S.; Andoralov, V.; Falk, M.; Reimann, C. T.; Ruzgas, T.; Srnec, M.; Ryde, U.; Rulisek, L., On the Possibility of Uphill Intramolecular Electron Transfer in Multicopper Oxidases: Electrochemical and Quantum Chemical Study of Bilirubin Oxidase. *Electroanalysis* **2012,** *24* (7), 1524-1540.
30. dos Santos, L.; Climent, V.; Blanford, C. F.; Armstrong, F. A., Mechanistic studies of the 'blue' Cu enzyme, bilirubin oxidase, as a highly efficient electrocatalyst for the oxygen reduction reaction. *Phys. Chem. Chem. Phys.* **2010,** *12* (42), 13962-13974.
31. Nemoto, M.; Sugihara, K.; Adachi, T.; Murata, K.; Shiraki, K.; Tsujimura, S., Effect of Electrolyte Ions on the Stability of Flavin Adenine Dinucleotide-Dependent Glucose Dehydrogenase. *ChemElectroChem* **2019,** *6* (4), 1028-1031.
32. Mazurenko, I.; Monsalve, K.; Rouhana, J.; Parent, P.; Laffon, C.; Le Goff, A.; Szunerits, S.; Boukherroub, R.; Giudici-Orticoni, M.-T.; Mano, N.; Lojou, E., How the intricate interactions between carbon nanotubes and two Bilirubin Oxidases control direct and mediated O_2 reduction. *ACS Appl. Mater. Interfaces* **2016,** *8* (35), 23074-23085.

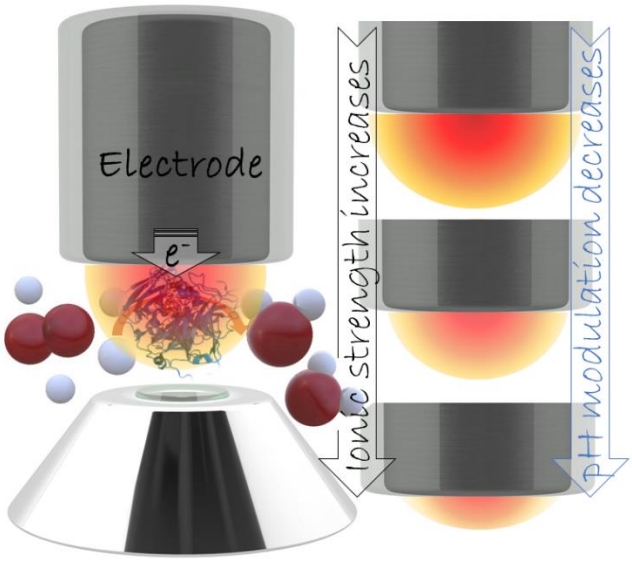

For Table of Contents only